IEEE Access
Multidisciplinary | Rapid Review | Open Access Journal

SPECIAL SECTION ON DEEP LEARNING ALGORITHMS FOR INTERNET OF MEDICAL THINGS

Received July 8, 2020, accepted July 16, 2020, date of publication July 20, 2020, date of current version July 30, 2020.

Digital Object Identifier 10.1109/ACCESS.2020.3010448

Computer-Aided Gastrointestinal Diseases Analysis From Wireless Capsule Endoscopy: A Framework of Best Features Selection

MUHAMMAD ATTIQUE KHAN[1], SEIFEDINE KADRY[2], (Senior Member, IEEE), MAJED ALHAISONI[3], YUNYOUNG NAM[4], (Member, IEEE), YUDONG ZHANG[5], (Senior Member, IEEE), VENKATESAN RAJINIKANTH[6], AND MUHAMMAD SHAHZAD SARFRAZ[7], (Member, IEEE)

[1]Department of Computer Science, HITEC University, Taxila 47080, Pakistan
[2]Department of Mathematics and Computer Science, Faculty of Science, Beirut Arab University, Beirut 11072809, Lebanon
[3]College of Computer Science and Engineering, University of Ha'il, Ha'il 55476, Saudi Arabia
[4]Department of Computer Science and Engineering, Soonchunhyang University, Asan 31538, South Korea
[5]Department of Informatics, University of Leicester, Leicester LE1 7RH, U.K.
[6]Department of Electronics and Instrumentation Engineering, St. Joseph's College of Engineering, Chennai 600119, India
[7]Department of Computer Science, National University of Computer and Emerging Sciences, Chiniot-Faisalabad Campus, Islamabad 44000, Pakistan

Corresponding authors: Muhammad Attique Khan (attique@ciitwah.edu.pk) and Yunyoung Nam (ynam@sch.ac.kr)

This research was supported by Korea Institute for Advancement of Technology (KIAT) grant funded by the Korea Government (MOTIE) (P0012724, The Competency Development Program for Industry Specialist) and the Soonchunhyang University Research Fund.

ABSTRACT The continuous improvements in the area of medical imaging, makes the patient monitoring a crucial concern. The internet of things (IoT) embedded in a medical technologies to collect data from human body through sensors, wireless connectivity etc. The junction of medicine and IT like medical informatics will transform healthcare, curbing cost, make more efficient, and saving lives. Various computerized techniques are implemented in the area of Artificial Intelligence (AI) for the application of medical imaging to diagnose the infected regions in the images and videos such as WCE and pathology. The famous stomach infections are ulcer, polyp, and bleeding. Stomach cancer is the most common infection and a leading cause of human deaths worldwide. In the USA, since 2019, a total of 27,510 new cases are reported including 17,230 men and 10,230 women. While the number of deaths is 11,140 consists of 6,800 men and 4,340 women. The manual diagnosis of these stomach infections is a difficult and agitated process therefore it is required to design a fully automated system using AI. In this article, we presented a fully automated system for stomach infection recognition based on deep learning features fusion and selection. In this design, ulcer images are assigned manually and support to a saliency-based method for ulcer detection. Later, pre-trained deep learning model named VGG16 is employing and re-trained using transfer learning. Features of re-trained model are extracted from two consecutive fully connected layers and fused by array-based approach. Besides, the best individuals are selected through the metaheuristic approach name PSO along mean value-based fitness function. The selected individuals are finally recognized through Cubic SVM. The experiments are conducted on Private collected dataset and achieved an accuracy of 98.4%, which is best as compared to existing state-of-the-art techniques.

INDEX TERMS Stomach diseases, WCE, saliency estimation, deep learning, features selection, features classification.

I. INTRODUCTION

In medical imaging, automatic detection and classification of cancers like skin cancer [1], [2], lungs cancer [3], brain tumor [4], stomach cancer [5] and few more are most important research topics from last few decades [6], [7]. From these, stomach is most common cancer name colon. The most common stomach infections are ulcer, bleeding, and polyps. These gastric infections have become a major cause of deaths of humans. A worldwide survey shows that colon cancer caused 525,000 mortalities, and 765,000 deaths occurred due to stomach cancer since 2017. In the United States, currently

The associate editor coordinating the review of this manuscript and approving it for publication was Wei Wei.

about 1.6 million people are facing bowel infections, and every year 0.2 million new cases are happening [8]. In the developing countries of the world, 694,000 deaths occurred due to colorectal cancer [9]. This is also known as bowel cancer. In 2015, 132,000 fresh cases of bowel cancer are happened according to an American cancer society [10]. In worldwide common cancers, esophageal cancer is at 7^{th} number [11]. In the global cancer deaths, stomach cancer is at 3^{rd} number [12].

WCE is the medical imaging technique to examine the gastrointestinal (GI) tract. This technique is extensively used in hospitals for the detection of gastric abnormalities such as ulcer, bleeding, and many more as shown in Figure 1 [13], [14]. A recent report shows that the treatment of about one million patients has been successfully done with WCE [15]. A small camera is used to capture the images of human gastrointestinal tract. Then the gastroenterologists analyze these WCE images, and it is a time taking procedure. About more than 50,000 images are produced during a WCE examination. A physician required two hours average to analyze these images, and a risk of false detection is also present [16].

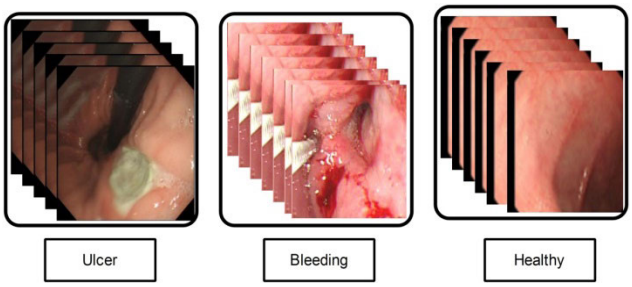

FIGURE 1. Sample frames of healthy and gastric abnormalities [14].

Many image processing researchers have developed the automated systems for the recognition of stomach infections from endoscopic images. These systems help in early detection of stomach diseases. The survival rate can be improved by diagnosing the gastric infections at early stage. The fundamental steps of the automated detection systems are features extraction, feature selection, and classification. Different methods for feature extraction utilized by the researchers are include point features [17], texture features [15], HOG features [18], and color features [19], [20]. Convolutional Neural Networks (CNNs) are combined with the handcrafted features to enhance the system's performance. Different CNN models such as AlexNet [21], VGG-16 [22], and ResNet [23] are used for the deep features extraction. The most important step in image processing is to extract and select the best features for classification. Most appropriate features produce the high accuracy results for the infection detection and classification.

II. RELATED WORK

Researchers have developed many automated detection and recognition systems. Mainly these are the supervised learning approaches that follows handcrafted and CNN features for detection and recognition of abnormalities in gastrointestinal tract. An esophageal cancer detection method is presented based on the Gabor features and Faster Region-Based CNN (Faster R-CNN). In this method, combined the handcrafted Gabor features with CNN descriptors [11]. Gabor features become more effective when combined with CNN features [24] and various studies have shown the effectiveness when handcrafted Gabor and deep features are combined [25]–[28]. A CNN based model is developed for the recognition of ulcer, polyp, and erosion. CNN features are used together with SVM for the detection of gastric infections. By using this technique, 80% accuracy was achieved [29]. This system utilized the fire segments from SqueezNet. This method reduces the size of network and achieves the accuracy of 88.90%. Billah *et al.* [30] combine the color wavelet features with CNN features. In classification phase, SVM is used to obtain the results. In [8], Geometric features are utilized from the segmented region of GI images. Then geometric features are combined with the features of VGG-19, and VGG-16. The deep features of VGG-19 and VGG-16 are fused based on the Euclidean Fisher Vector method.

A color transformation based technique is presented in [31]. HSI and YIQ transformation is applied on RGB images and calculate the maximum and minimum pixel values. Then Local Binary Pattern (LBP), and Gray Level Co-occurrences Matrices (GLCM) features are extracted and fused with the color-based features and the final vector fed to the multi-layer perceptron. This technique detects and classifies the stomach infections. A model is proposed for ulcer detection based on YIQ color transformation [32]. This method utilized the Y plane and SVM is used in classification phase. Suman *et al.* [19] developed a statistical color features based technique for automatic detection of gastric bleeding. A two phase model is introduced for automated detection of ulcer [33]. In first step, a super pixels-based saliency method is utilized, which identify the infected region. In second step, saliency based max pooling (SMP) technique is introduced. The SMP method then combines with locality constrained linear coding (LLC) and obtains the 92.65% of classification accuracy. For the classification of bleeding, polyp, and ulcer K-mean clustering technique was utilized and achieve 88.61% of accuracy. A method was developed based on texture features for the classification of ulcer and non-ulcer. The final feature vector then fed to the SVM classifier and achieved 94.16% of accuracy [10]. Fan *et al.* [16] introduced a stomach diseases recognition system based on LBP, and Scale-Invariant Feature Transform (SIFT) features.

Discrete Wavelet Transform (DWT), variance, and LBP features are extracted and classified using SVM for the detection of colon infections. Texture information is calculated from these features, and SVM classifier is used to obtain the classification results [34]. Bag of visual Words (BoW) is generated from the features extracted from different color spaces and color histograms for bleeding detection [35]. Features of

pre-trained networks such as Inception-V3, and VGGNet are extracted and fused with the baseline features. This method achieved the 96.1% classification accuracy on SVM [36]. A similar method is proposed utilizing ResNet50 features. Feature vector fed to the logistic model tree (LMT) for classification, and 95.7% of accuracy is achieved [37]. A technique is introduced based on color and statistical texture features for detection of GI tract infections [38]. HSI and LAB color transformations are used to detect the bleeding area in WCE images. These color spaces are helpful in bleeding detection. Classification results are enhanced by using multi perceptron learning approach [39]. Shape, texture, and color features were utilized in different studies to detect the abnormal regions [40], [41]. Fisher scoring method was applied to select the feature set with maximum information, extracted from HSV color transformation and texture features. Researchers classify the ulcer and bleeding images using multilayered neural network [42]. Two SVM classifiers based on RGB and HSV color spaces were fused to build an automated detection system [43]. This classifier fusion technique achieved the classification accuracy of 95%.

III. CHALLENGES AND CONTRIBUTIONS

In the above listed techniques, it is observed that the most of recent methods follows the fusion process of handcrafted and CNN features. However, this process increases the overall system execution time. Moreover, it is also noted that the existing techniques decreases the classification accuracy in the process of raw images for features extraction. For example, the pixels values of ulcer and original images are almost similar except infected region pixels. Therefore, it is a solution to first extract the ulcer regions from the original frames and then extract its features. Few other challenges are inconsistency of ulcer regions and selection of irrelevant features which cause a problem in accurate infection classification. In this article, a new method is proposed for automated gastrointestinal infections recognition using WCE imaging modality. Major contributions are:

a) A dark channel along with de-correlation formulation based approach is designed to improve the pixel range of ulcer region.
b) An optimized saliency based method is adopted along with few morphological operations for ulcer detection.
c) Using pre-trained deep learning model named VGG16 and extract features using transfer learning. Features are computed from two sequential layers and fused using array-based method.
d) Best features are selected through PSO-GM meta-heuristic approach and classify selected features using Cubic SVM. The results of both fusion and selection process are computed and analyzed in terms of confusion matrices and graphs.

IV. PROPOSED METHODOLOGY

In this article, a new automated system is proposed for gastrointestinal infections recognition from WCE imaging modality. The proposed system includes few famous steps including preprocessing of ulcer frames through dark channel prior and decorrelation based ulcer visibility improvement, segmentation of ulcer using optimized saliency based method along with morphological operations, deep learning features extraction, selection of best features, and finally classification of selected features. These steps are clearly illustrated in Figure 2. The detail of each step is given below.

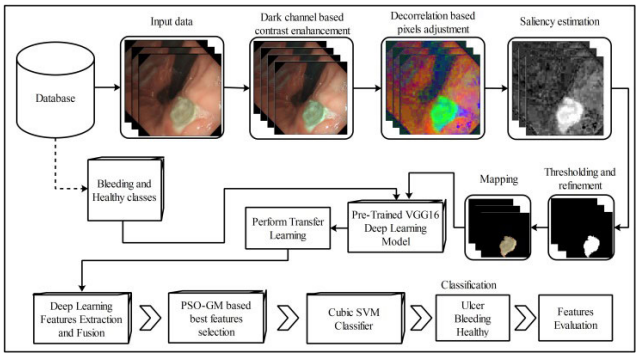

FIGURE 2. Detailed flow diagram of gastrointestinal infections recognition.

A. DATA ACQUISITION

Image acquisition anticipates taking images for validation of the proposed method. In this work, WCE imaging modality is employed for the detection and recognition of stomach infections. These images are obtained from the CUI Wah database [31], which includes a total of 6000 RGB images of WCE modality. A few sample images are also illustrated in Figure 1. These images further include ulcer, bleeding, and normal where apiece category includes 2000 images. In this dataset, ulcer images are separate manually and further utilized for segmentation while the bleeding and normal images are directly supported to the feature extraction step as shown in Figure 2.

B. ULCER DETECTION

In the ulcer detection step, the following process is followed- i) dark channel based contrast enhancement; ii) implementation of decorrelation formulation on dark channel enhanced image, iii) implement an existing saliency method on decorrelated image, and iv) perform morphological operations for final refinement. Improve the visibility of an image at the initial stage is an important step to get better detection and relevant features of an infected region. As shown in Figure 3 (a), the original WCE images have dark effects on ulcer regions which mean that the pixel range of infected part is towards 0. For this purpose, we implement a haze reduction based approach [44].

Let, we have original WCE frames denotes by Δ and one image denoted by $\varphi\,(x, y)$ of dimension $512 \times 512 \times 3$ where $N = 512$, $M = 512$, and three channels R, G, and B, respectively. According to [45], haze formulation is defined

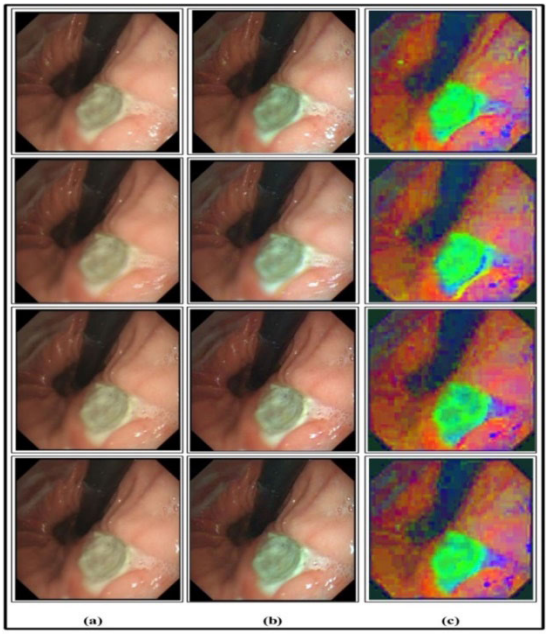

FIGURE 3. Dark channel enhancement and decorrelation formulation effects- a) original WCE image; b) dark channel enhanced image; c) formulation of decorrelation effects.

as:

$$\tilde{\varphi}(f) = J(f)\, t(f) + A(1 - t(f)) \tag{1}$$

where, $f \in (x, y)$, $\tilde{\varphi}(f)$ is observed intensity, J denotes the scene radiance, global air brightness is denoted by A, and $t(f)$ represents the medium transmission of light, respectively. The problem of radiance is removal is key issue in this work which is defined through following formulation:

$$J(f) = \frac{(\tilde{\varphi}(f) - A)}{(\max(t(f), t_0))} + A \tag{2}$$

The effects of this formulation are illustrated in Figure 3(b).

Later, the decorrelation formulation is employed on $J(f)$ to highlight the ulcer regions. Mathematically, the formulation of decorrelation is defined as:

$$\beta = \tau \times (\alpha - \mu) + \mu_t \tag{3}$$

where, β denotes the corresponding pixel in resultant image, α denotes $n \times 1$ band vector, τ is an $n \times n$ band vectors, μ is a mean and μ_t denotes the target mean of each sub-bands, respectively. Later, compute the correlation as:

$$Cor = inv(\sigma) \times Cov \times inv(\sigma) \tag{4}$$

where, $\sigma(k, k) = \sqrt{Cov(k, k)}$ and $k = 1, 2, 3, \ldots, n\_bands$. By employing these n_bands, the stretch function is formulated as:

$$S_f(k, k) = \frac{1}{\sqrt{\lambda(k, k)}} \tag{5}$$

$$\tau = \sigma_t O_m S (O_m)' \tag{6}$$

where, S represent a diagonal matrix, λ is a diagonal matrix of Eigen Values (EV), and O_m is an orthogonal matrix, respectively. At the end, all these notations are employed in β to compute final output as:

$$\beta = \mu_t + \sigma_t O_m S (O_m)' inv(\sigma) \times (\alpha - \mu) \tag{7}$$

The resultant outputs of this formulation in the form of visual effects are shown in Figure 3 (c). In this figure, it is clearly presented that after implementation of decorrelation formulation; the ulcer region is clearly highlighted. After that, the ulcer is segmented by using an existing saliency based approach name histogram based contrast pixels clustering [46]. As we have resultant decorrelated image β where $\beta \in \beta_1(x, y)$ which is utilized for computing the distance among pixels of image as:

$$Sal(\beta_q) = \sum\nolimits_{\forall \beta_i \in \beta} d(\beta_q, \beta_i) \tag{8}$$

where, $d(\beta_q, \beta_i)$ denotes the color distance among pixels β_q and β_i in image β. This expression computes the distance among image pixels which later grouped same type of pixels into number of clusters like pixels which are range of green values and any others as follows:

$$Sal(cl) = \sum\nolimits_{k=1}^{K} p_j d(cl, c_k) \tag{9}$$

where, p_j denotes the probability of pixels color c_k in image β. This expression return a pixels based saliency map as shown in Figure 4 (b). Furthermore, convert this saliency mapped image into binary format by employing following threshold function.

$$Th(x, y) = \begin{cases} 1 & if\ Sal(cl) \geq Thr \\ 0 & Otherwise \end{cases} \tag{10}$$

where, $Th(x, y)$ denotes the binary image as shown in Figure 4 (c) and Thr is a threshold value which range is between 0.683 to 0.719. These binary images are further refined by applying morphological operations such as closing and dilation, and its effects are illustrated in Figure 4(d).

C. DEEP LEARNING FEATURES

Classification is a key challenge in machine learning but the performance of this always depends on the nature of input data like features [47], [48]. The power of ML depends on the number of training data; however, a lot of samples are noisy and irrelevant which generates noisy and inappropriate features [49]. Through, these features, the performance of a system is decreased which is a key issue in this area [50], [51]. In medical imaging, the selection of best features is more important for classification [52]. The key challenge in the classification phase is how to select the most discriminant features for the final classification. In this work, we are using deep learning features. A pre-trained deep learning model named VGG16 is employing and re-trained with the help of transfer learning on collected WCE dataset. Later, an important texture features are concatenated with deep features and applied optimization of features using PSI-GM approach. The selected features are finally classified using Cubic SVM classifier. A flow diagram is showing in Figure 5.

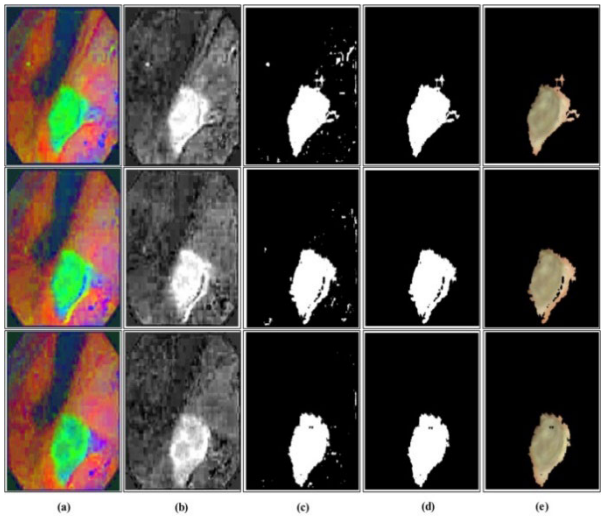

FIGURE 4. Ulcer detection results- (a) implementation of decorrelation formulation as an input; (b) saliency estimation; (c) binary image through thresholding function; (d) refinement function and morphological operations based effects, and (e) mapped results.

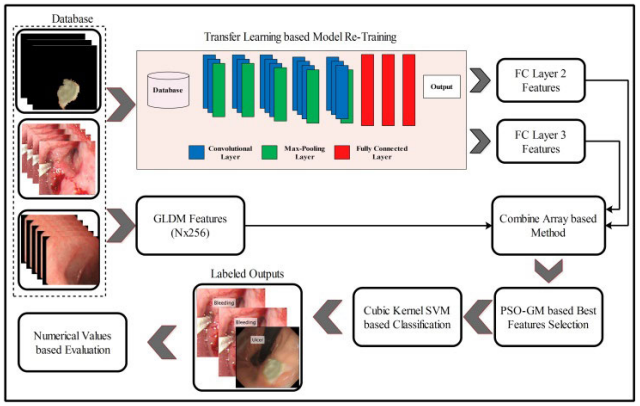

FIGURE 5. Overview of extracted features and best selected features for recognition.

1) PRE-TRAINED DEEP LEARNING MODEL

A pre-trained CNN model named VGG16 [] is employing in this work for deep learning features. Originally, this model consists of five convolutional layers and 3 fully connected (FC) layers along with a Softmax layer for final classification. The layers are max pooling and ReLu. Between FC layers, a dropout layer is added of value 0.5. This model take an input image of size $224 \times 224 \times 3$. Initially, input image is passed in first convolutional layer. In this layer image features are extracted and passed in the next successive layer as shown in Figure 6. Mathematically, the convolutional layer is defined as follows:

$$\lambda_{(t)}^{(k)} = \sigma\left(\psi^{(k)}\lambda^{(k-1)}(t) - \beta^{(k)}\right) \tag{11}$$

where, $k = 1, 2, 3, ..K$, $\psi^{(k)} = \left(w_{j-k}^{(i)}\right)$ is a $d_i \times d_{i-1}$ convolutional matrix, σ act as a vector component and defined as a ReLu activation function.

$$\sigma(k) = \max(\mathrm{k}, 0), \quad k \in \mathbb{R} \tag{12}$$

The β represent as a bias vector and defined as- $\beta = \{d_i \times d_{i-1}\}$. Another layer name max pooling is also added in this network to resolve the problem of underflow. Later on, the most important layer named FC is added. In this layer, the information is extracted into a one-dimensional. The features of this layer are used for classification through Softmax layer. A main architecture of VGG16 is showing in Figure 6.

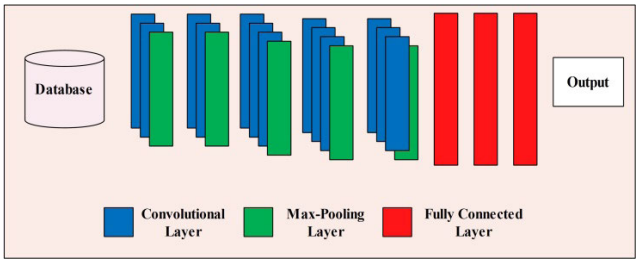

FIGURE 6. Pre-trained VGG16 deep learning model.

2) TRANSFER LEARNING BASED FEATURE EXTRACTION

In this article, we are employing transfer learning to re-train this model on WCE images. In the TL, the same parameters of original model are utilized to train a new model. The main purpose of TL is to solve the problem of much time for training a new model from scratch. Based on TL based training, it is easy to train a model with less computational time. After retraining this model on WCE images, the activation is employing on last two FC layers for features extraction. The size of resultant vector of each layer is 1×4096 and 1×1000, respectively. For N images, the resultant vectors length is $N \times 4096$ and $N \times 1000$, respectively.

3) GRAY LEVEL DIFFERENCE MATRIX (GLDM)

The GLDM features [53] are represented as absolute difference among two gray level pixels of an image. In this method, three core parameters are required such as difference, distance, and angle. Mathematically, it can be formulated as:

$$D_v = (\nu_k, \nu_l) \tag{13}$$

$$I_n(k, l) = |I_n(k, l) - I_n(k + \nu_k, l + \nu_l)| \tag{14}$$

$$(k, D_v) = Prob(I_{n(0)}(k, l) = 1) \tag{15}$$

where, $I_n(k, l)$ denotes the image intensity values and (k, D_v) represent estimated probability density function, respectively. For extraction of GLDM features, the following parameters are initialized: difference is 2, distance is 1, and angle is 0^0. In the output, a resultant vector is returned of matrix dimension $256 \times pd$ where $pd \in (1, 2, 3, 4)$ and we select $pd = 2$.

D. FEATURES FUSION AND SELECTION

After that, a simple array based method is proposed to combine both sequential layer features in one matrix. The main purpose of fusion process is to obtain more informative feature vector for best classification. Mathematically, this process is explained below:

Let ΔX_1 denotes feature vector of FC layer two of dimension $N \times 4096$, ΔX_2 denotes feature vector of FC layer three of dimension $N \times 1000$, and ΔX_3 denotes feature vector of GLDM features of dimension $N \times 256$. Suppose ΔX_N is a resultant feature matrix of dimension $N \times K$, where K denotes fused features. Hence the initial length of features is depends on the all three vectors sum and computed as:

$$\sum(\Delta) = \sum_{i=1}^{3} \sum_{j=1}^{N} \left(\Delta X_i^j\right) \tag{16}$$

Based on the size of $\sum(\Delta)$, an array is initialized and place features as:

$$\Delta X_N = (\Delta X_1, \Delta X_2) \tag{17}$$

$$\Delta X_N = \begin{pmatrix} \Delta X_1 \\ \Delta X_2 \\ \Delta X_3 \end{pmatrix}_{N \times \sum(\Delta)} \tag{18}$$

Finally, the fused features are optimized using evolutionary search method named PSO [54] along with grand mean fitness function. PSO have two major benefits and it is a motivation of chosen- convergence speed is fast and less computational cost. Mathematically, PSO is defined as follows:

$$Vl_{i,j} = Vl_{i,j} + c_1 r_{1,j} \left(\varphi_{i,j}^{pbt} - \varphi_{i,j}\right) + c_2 r_{2,j} \left(\varphi_j^{gbt} - \varphi_{i,j}\right) \tag{19}$$

where, φ_i and Vl_i denotes position vectors and velocity vectors, respectively. These vectors are defined as:

$$\varphi_i = \left(\varphi_{i,1}, \varphi_{i,2}, \ldots, \varphi_{i,n}\right)^T \tag{20}$$

$$Vl_i = \left(Vl_{i,1}, Vl_{i,2}, \ldots, Vl_{i,n}\right)^T \tag{21}$$

The historical best position and population historical best position is denoted by $\varphi_{i,j}^{pbt}$ and φ_j^{gbt}, and initialized as follows:

$$\varphi_{i,j}^{pbt} = \left(\varphi_{i,1}^{pbt}, \varphi_{i,2}^{pbt}, \ldots., \varphi_{i,n}^{pbt}\right)^T \tag{22}$$

$$\varphi_j^{gbt} = \left(\varphi_1^{gbt}, \varphi_2^{gbt}, \ldots., \varphi_n^{gbt}\right)^T \tag{23}$$

In each generation, particles are evaluated by a fitness function. The main purpose of fitness function is to give the best solution for final classification. A grand mean based fitness function is employing in this work.

$$Fitness = \sqrt{\sum_{i=1}^{C} \left\{(\mu_i - \mu_0)^t \left((\mu_i - \mu_0)\right)\right\}} \tag{24}$$

where, μ_i denotes corresponding class mean value and μ_0 denotes grand mean of whole feature space. Based on this, if fitness value is greater than pbest and gbest, then it will be updated. After that One-against-All SVM is utilized of Cubic kernel function for the classification of these best features. The performance of Cubic SVM is compared with few other classification algorithms as shown in Figure 7.

Model	Description	Model	Description
Cubic SVM	Kernel Function: Cubic Kernel Scale: Automatic Box Constraint Level: 1 Multiclass Method: one-vs-one Standardize Data: true	Coarse Gaussian SVM	Kernel Function: Gaussian Kernel Scale: 140 Box Constraint Level: 1 Multiclass Method: one-vs-one Standardize Data: true
Linear SVM	Kernel Function: Linear Kernel Scale: Automatic Box Constraint Level: 1 Multiclass Method: one-vs-one Standardize Data: true	Fine KNN	No. of Neighbors: 1 Distance Metric: Euclidean Distance Weight: Equal Standardize Data: true
Quadratic SVM	Kernel Function: Quadratic Kernel Scale: Automatic Box Constraint Level: 1 Multiclass Method: one-vs-one Standardize Data: true	Boosted Trees	Ensemble Method: AdaBoost Learner Type: Decision Tree Maximum No. of Splits: 20 No. of Learners: 30 Learning Rate: 0.1
Medium Gaussian SVM	Kernel Function: Gaussian Kernel Scale: 35 Box Constraint Level: 1 Multiclass Method: one-vs-one Standardize Data: true	Fine Tree	Maximum No. of Splits: 100 Split Criterion: Gini's Diversity Index Surrogate Decision Splits: Off
Medium Tree	Maximum No. of Splits: 20 Split Criterion: Gini's Diversity Index Surrogate Decision Splits: Off	Coarse Tree	Maximum No. of Splits: 4 Split Criterion: Gini's Diversity Index Surrogate Decision Splits: Off

FIGURE 7. Description of selected classifiers for experimental process.

V. RESULTS AND ANALYSIS

In the experimental process, a Privately collected dataset is employed as a detailed description is provided in Section 4.1. The images in this dataset are complex like low brightness of ulcer regions and similarity of pixels. In the evaluation step, the performance of Cubic SVM is compared with a few other classification techniques as illustrated in Figure 7. A 10-Fold cross validation is performed for both training and testing data [55], where selected ratio is 70, 30. For performance analysis, standard parameters are employed- sensitivity (Sen), precision (Pre), F1 Score (F1-S), area under the curve (AUC), FP rate (FPR), and accuracy. All simulations were employed on MATLAB Tool with Deep Learning (DL) toolbox name Matconvnet. This tool was employed for CNN feature extraction.

A. NUMERICAL AND VISUAL RESULTS

The numerical results of this work are presented in this section. The results are acquired in two different steps. In the first step, fusion of extracted features based experiment was performed and results are given in Table 1. In this table, it is clearly illustrated that the recognition results on CSVM are best in the form of standard calculated parameters such as Sen (96.42%), Pre (96.20%), F1-S (96.31%), AUC (0.992), FPR (0.019), and accuracy is 96.50%, respectively. In Figure 8, the performance of CSVM can be confirmed by calculating the true positive rates (TPR). In this figure, it is indicated that the normal class gives maximum of 97% TPR. Compared with other classification techniques, it is observed

TABLE 1. Proposed features fusion based classification results on Private collected dataset.

Classifier	Calculated Parameters					
	Sen (%)	Pre (%)	F1-S (%)	AUC	FPR	Accuracy (%)
LSVM	93.30	93.10	93.20	0.972	0.031	93.40
QSVM	94.40	94.18	94.29	0.986	0.029	94.92
CSVM	**96.42**	**96.20**	**96.31**	**0.992**	**0.019**	**96.50**
MGSVM	95.90	95.84	95.87	0.990	0.022	96.00
Co-SVM	89.96	89.92	89.94	0.969	0.044	90.14
FKNN	91.10	91.06	91.08	0.975	0.042	91.40
EBT	86.40	86.28	86.34	0.952	0.066	86.80
DT	87.23	87.10	87.16	0.960	0.062	87.42

Disease Type	Disease Type		
	Bleeding	Normal	Ulcer
Bleeding	96%	2%	2%
Normal	1%	97%	2%
Ulcer		3.5%	96.5%

FIGURE 8. Confusion matrix of CSVM for proposed features fusion process.

TABLE 2. Proposed features selection based classification results on Private collected dataset.

Classifier	Calculated Parameters					
	Sen (%)	Pre (%)	F1-S (%)	AUC	FPR	Accuracy (%)
LSVM	97.00	96.60	96.80	0.997	0.017	96.60
QSVM	98.01	98.04	98.02	1.00	0.013	97.90
CSVM	**98.33**	**98.36**	**98.34**	**1.00**	**0.007**	**98.40**
MGSVM	98.00	97.90	97.95	1.00	0.010	98.20
Co-SVM	94.00	94.00	94.00	0.990	0.033	93.80
FKNN	92.90	92.64	92.77	0.986	0.037	93.00
EBT	90.94	90.72	90.83	0.963	0.048	91.20
DT	91.36	91.00	91.18	0.970	0.044	91.60

Disease Type	Disease Type		
	Bleeding	Normal	Ulcer
Bleeding	99%	1%	1%
Normal	1%	98%	1%
Ulcer	1%	1%	98%

FIGURE 9. Confusion matrix of CSVM for proposed features selection process.

from Table 1 that the second best performance in the fusion process is 96% (accuracy) which is achieved on MGSVM. While, the lowest attained accuracy is 86.80% for EBT classifier. On the remaining classifiers such as LSVM, QSVM, Co-SVM, FKNN, EBT, and DT, the accuracy performance is 93.40%, 94.92%, 90.14%, 91.40%, 86.80%, and 87.42%, respectively. Overall, it is observed that the fusion of all calculated features was performed well.

In the second step, the best selected features based on PSO-GM approach are employed for experimental process and results are given in Table 2. In this table, it is clearly illustrated that the recognition results on CSVM are best in the form of standard calculated parameters such as Sen (98.33%), Pre (98.36%), F1-S (98.34%), AUC (1.00), FPR (0.007), and accuracy is 98.40%, respectively. In Figure 9, the performance of CSVM can be confirmed by calculating the true positive rates (TPR). Compared with the other classification techniques, it is observed from Table 2 that the second best performance in the fusion process is 98.20% (accuracy) which is achieved on MGSVM. While, the lowest attained accuracy is 91.20% for EBT classifier. On the remaining classifiers such as LSVM, QSVM, Co-SVM, FKNN, EBT, and DT, the accuracy performance is 96.60%, 97.90%, 93.80%, 93.00%, 91.20%, and 91.60%, respectively. Overall, it is observed that the selection of best features through proposed approach gives sufficient accuracy on all listed classifiers.

B. DISCUSSION AND COMPARISON

Initially, the visual analysis is performed of proposed numerical results as presented in Table 1 and 2. From these tables, it is observed that the selection of best features through proposed PSO-GM based method given better results as compare to fusion process. The comparison in the form of fused features based accuracy and selection based accuracy is plotted in Figure 10. In this figure, it is observed that the selection accuracy is almost 3% to 4% increases as compared to fused vector results. Furthermore, the visual effects of each step as listed in Figure 2 are also shown such as in Figure 3, the effects of contrast improvement and implementation of de-correlation formulation are illustrated. Later on, through saliency based ulcer segmentation is performed that further refined through morphological operations as shown in Figure 10. In this figure, the final output mapped results are put in features extraction step instead of whole ulcer image. The purpose of this step is to get the more relevant features which are dissimilar as compare to normal image features. The whole architecture of features based recognition is shown in Figure 5. Overall analysis, it is observed that the selection of best features based recognition process gives better accuracy on CSVM as compared to other classifiers. Moreover, it is also observed from the results, given in Table 1 and 2, the accuracy of fused vector is lesser related to selection vector.

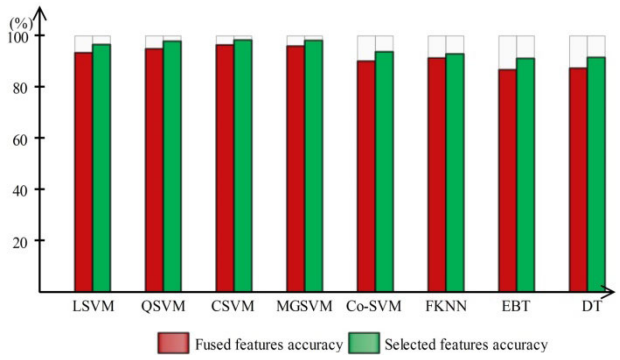

FIGURE 10. Proposed features based accuracy comparison on Private dataset.

In the addition, we compare the feature fusion and selection results with few deep learning models. In this comparison, we extract features from original models and perform classification without any selection approach. Results are plotted in Figure 11. In this figure, it is showing that the feature selection process gives improved performance as compared to other deep learning models. Also, this figure shows the choice of VGG16 pre-trained model for deep feature extraction for WCE images.

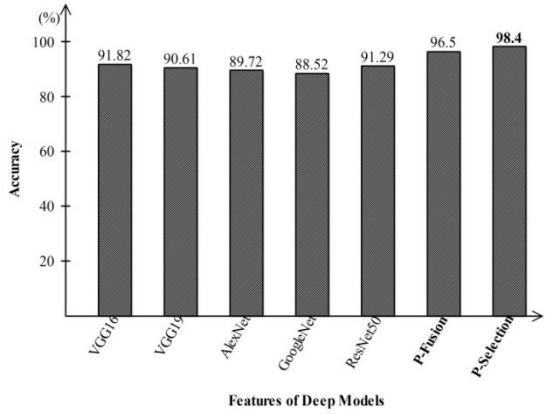

FIGURE 11. Comparison of proposed results with existing deep learning models for WCE images.

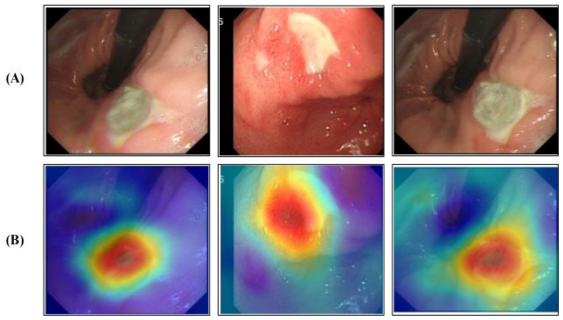

FIGURE 12. Comparison of proposed results with existing deep learning models for WCE images.

The visualization of selected deep feature is illustrated in Figure 12. In the last, we compare the proposed fusion and selection results with few latest techniques to further authenticate the performance of proposed architecture. In [20], authors achieved an accuracy of 97.89%. Liaqat *et al.* [14] attained accuracy of 98.49% on same dataset while our method achieved an accuracy of 98.40% where number of images in the updated dataset was higher than [14]. From the results, it is clearly illustrated the achievement of proposed scheme.

VI. CONCLUSION

A fully automated CAD system is proposed in this work for stomach infection diagnosis and classification using deep learning. In the proposed design, initially, an ulcer is detected through a saliency-based method and next step deep learning and GLDM features are extracted. The array based approach is employing to fused these features and optimize the resultant vector using PSO-GM evolutionary approach. The selected features are classified using Multi-class Cubic SVM and achieved an accuracy of 98.40%. Based on the results, it is concluded that the process of ulcer detection instead of direct used for features extraction gives most discriminative features as compared to features computed through original images. However, it is also noted that this process increase the system computational time which is a key limitation of this work. Besides, it is concluded that the reduction of fused features through Meta heuristic approach returns more informative features which helps in better recognition performance. The main limitations of this work are- (i) incorrect segmentation of ulcer regions create a problem in false training of a deep learning model and also responsible for extracting irrelevant features, (ii) selection of features using evolutionary techniques consume higher time as compare to heuristic techniques. In the future studies, our focus will be on minimizing the computational time.

REFERENCES

[1] M. A. Khan, M. Sharif, T. Akram, S. A. C. Bukhari, and R. S. Nayak, "Developed Newton-raphson based deep features selection framework for skin lesion recognition," *Pattern Recognit. Lett.*, vol. 129, pp. 293–303, Jan. 2020.

[2] T. Saba, M. A. Khan, A. Rehman, and S. L. Marie-Sainte, "Region extraction and classification of skin cancer: A heterogeneous framework of deep CNN features fusion and reduction," *J. Med. Syst.*, vol. 43, no. 9, p. 289, Sep. 2019.

[3] M. A. Khan, S. Rubab, A. Kashif, M. I. Sharif, N. Muhammad, J. H. Shah, Y.-D. Zhang, and S. C. Satapathy, "Lungs cancer classification from CT images: An integrated design of contrast based classical features fusion and selection," *Pattern Recognit. Lett.*, vol. 129, pp. 77–85, Jan. 2020.

[4] M. I. Sharif, J. P. Li, M. A. Khan, and M. A. Saleem, "Active deep neural network features selection for segmentation and recognition of brain tumors using MRI images," *Pattern Recognit. Lett.*, vol. 129, pp. 181–189, Jan. 2020.

[5] M. A. Khan, M. Sharif, T. Akram, M. Yasmin, and R. S. Nayak, "Stomach deformities recognition using rank-based deep features selection," *J. Med. Syst.*, vol. 43, no. 12, p. 329, Dec. 2019.

[6] M. A. Khan, I. U. Lali, A. Rehman, M. Ishaq, M. Sharif, T. Saba, S. Zahoor, and T. Akram, "Brain tumor detection and classification: A framework of marker-based watershed algorithm and multilevel priority features selection," *Microsc. Res. Technique*, vol. 82, no. 6, pp. 909–922, Jun. 2019.

[7] M. A. Khan, T. Akram, M. Sharif, K. Javed, M. Rashid, and S. A. C. Bukhari, "An integrated framework of skin lesion detection and recognition through saliency method and optimal deep neural network features selection," *Neural Comput. Appl.*, pp. 1–20, Nov. 2019.
[8] M. Sharif, M. A. Khan, M. Rashid, M. Yasmin, F. Afza, and U. J. Tanik, "Deep CNN and geometric features-based gastrointestinal tract diseases detection and classification from wireless capsule endoscopy images," *J. Experim. Theor. Artif. Intell.*, pp. 1–23, Feb. 2019.
[9] R. L. Siegel, K. D. Miller, S. A. Fedewa, D. J. Ahnen, R. G. S. Meester, A. Barzi, and A. Jemal, "Colorectal cancer statistics, 2017," *CA, A Cancer J. Clinicians*, vol. 67, no. 3, pp. 177–193, May 2017.
[10] Y. Yuan and M. Q.-H. Meng, "Deep learning for polyp recognition in wireless capsule endoscopy images," *Med. Phys.*, vol. 44, no. 4, pp. 1379–1389, Apr. 2017.
[11] N. Ghatwary, X. Ye, and M. Zolgharni, "Esophageal abnormality detection using DenseNet based faster R-CNN with Gabor features," *IEEE Access*, vol. 7, pp. 84374–84385, 2019.
[12] J. H. Lee, Y. J. Kim, Y. W. Kim, S. Park, Y.-I. Choi, Y. J. Kim, D. K. Park, K. G. Kim, and Jun-Won Chung, "Spotting malignancies from gastric endoscopic images using deep learning," *Surgical Endoscopy*, vol. 33, pp. 3790–3797, Feb. 2019.
[13] K. Mergener, "Update on the use of capsule endoscopy," *Gastroenterology hepatology*, vol. 4, p. 107, Feb. 2008.
[14] A. Liaqat, M. A. Khan, J. H. Shah, M. Sharif, M. Yasmin, and S. L. Fernandes, "Automated ulcer and bleeding classification from WCE images using multiple features fusion and selection," *J. Mech. Med. Biol.*, vol. 18, no. 4, Jun. 2018, Art. no. 1850038.
[15] B. Li and M. Q.-H. Meng, "Tumor recognition in wireless capsule endoscopy images using textural features and SVM-based feature selection," *IEEE Trans. Inf. Technol. Biomed.*, vol. 16, no. 3, pp. 323–329, May 2012.
[16] S. Fan, L. Xu, Y. Fan, K. Wei, and L. Li, "Computer-aided detection of small intestinal ulcer and erosion in wireless capsule endoscopy images," *Phys. Med. Biol.*, vol. 63, no. 16, Aug. 2018, Art. no. 165001.
[17] E. Tuba, M. Tuba, and R. Jovanovic, "An algorithm for automated segmentation for bleeding detection in endoscopic images," in *Proc. Int. Joint Conf. Neural Netw. (IJCNN)*, May 2017, pp. 4579–4586.
[18] S. Charfi and M. El Ansari, "Computer-aided diagnosis system for ulcer detection in wireless capsule endoscopy videos," in *Proc. Int. Conf. Adv. Technol. Signal Image Process. (ATSIP)*, May 2017, pp. 1–5.
[19] S. Suman, F. A. B. Hussin, A. S. Malik, K. Pogorelov, M. Riegler, S. H. Ho, I. Hilmi, and K. L. Goh, "Detection and classification of bleeding region in WCE images using color feature," in *Proc. 15th Int. Workshop Content-Based Multimedia Indexing CBMI*, 2017, p. 17.
[20] S. Suman, F. Hussin, A. Malik, S. Ho, I. Hilmi, A. Leow, and K.-L. Goh, "Feature selection and classification of ulcerated lesions using statistical analysis for WCE images," *Appl. Sci.*, vol. 7, no. 10, p. 1097, Oct. 2017.
[21] A. Krizhevsky, I. Sutskever, and G. E. Hinton, "ImageNet classification with deep convolutional neural networks," in *Proc. Adv. Neural Inf. Process. Syst. (NIPS)*, 2012, pp. 1097–1105.
[22] K. Simonyan and A. Zisserman, "Very deep convolutional networks for large-scale image recognition," 2014, *arXiv:1409.1556*. [Online]. Available: http://arxiv.org/abs/1409.1556
[23] K. He, X. Zhang, S. Ren, and J. Sun, "Deep residual learning for image recognition," in *Proc. IEEE Conf. Comput. Vis. Pattern Recognit. (CVPR)*, Jun. 2016, pp. 770–778.
[24] Q. Shi, W. Li, F. Zhang, W. Hu, X. Sun, and L. Gao, "Deep CNN with multi-scale rotation invariance features for ship classification," *IEEE Access*, vol. 6, pp. 38656–38668, 2018.
[25] S. Luan, C. Chen, B. Zhang, J. Han, and J. Liu, "Gabor convolutional networks," *IEEE Trans. Image Process.*, vol. 27, no. 9, pp. 4357–4366, Sep. 2018.
[26] H. Yao, L. Chuyi, H. Dan, and Y. Weiyu, "Gabor feature based convolutional neural network for object recognition in natural scene," in *Proc. 3rd Int. Conf. Inf. Sci. Control Eng. (ICISCE)*, Jul. 2016, pp. 386–390.
[27] B. Kwolek, "Face detection using convolutional neural networks and Gabor filters," in *Proc. Int. Conf. Artif. Neural Netw.*, 2005, pp. 551–556.
[28] Y. Chen, L. Zhu, P. Ghamisi, X. Jia, G. Li, and L. Tang, "Hyperspectral images classification with Gabor filtering and convolutional neural network," *IEEE Geosci. Remote Sens. Lett.*, vol. 14, no. 12, pp. 2355–2359, Dec. 2017.
[29] X. Zhang, W. Hu, F. Chen, J. Liu, Y. Yang, L. Wang, H. Duan, and J. Si, "Gastric precancerous diseases classification using CNN with a concise model," *PLoS ONE*, vol. 12, no. 9, Sep. 2017, Art. no. e0185508.
[30] M. Billah, S. Waheed, and M. M. Rahman, "An automatic gastrointestinal polyp detection system in video endoscopy using fusion of color wavelet and convolutional neural network features," *Int. J. Biomed. Imag.*, vol. 2017, pp. 1–9, Aug. 2017.
[31] M. A. Khan, M. Rashid, M. Sharif, K. Javed, and T. Akram, "Classification of gastrointestinal diseases of stomach from WCE using improved saliency-based method and discriminant features selection," *Multimedia Tools Appl.*, vol. 78, pp. 27743–27770, Jun. 2019.
[32] A. K. Kundu, A. Bhattacharjee, S. A. Fattah, and C. Shahnaz, "An automatic ulcer detection scheme using histogram in YIQ domain from wireless capsule endoscopy images," in *Proc. IEEE Region Conf. TENCON*, Nov. 2017, pp. 1300–1303.
[33] Y. Yuan, J. Wang, B. Li, and M. Q.-H. Meng, "Saliency based ulcer detection for wireless capsule endoscopy diagnosis," *IEEE Trans. Med. Imag.*, vol. 34, no. 10, pp. 2046–2057, Oct. 2015.
[34] S. Charfi and M. E. Ansari, "Computer-aided diagnosis system for colon abnormalities detection in wireless capsule endoscopy images," *Multimedia Tools Appl.*, vol. 77, no. 3, pp. 4047–4064, Feb. 2018.
[35] Y. Yuan, B. Li, and M. Q.-H. Meng, "Bleeding frame and region detection in the wireless capsule endoscopy video," *IEEE J. Biomed. Health Informat.*, vol. 20, no. 2, pp. 624–630, Mar. 2016.
[36] T. Agrawal, R. Gupta, S. Sahu, and C. Y. Espy-Wilson, "SCL-UMD at the medico task-MediaEval 2017: Transfer learning based classification of medical images," in *MediaEval*, 2017.
[37] K. Pogorelov, K. R.Randel, C. Griwodz, S. L. Eskeland, T. de Lange, D. Johansen, C. Spampinato, D. T. Dang-Nguyen, M. Lux, P. T. Schmidt, and M. Riegler, "Kvasir: A multi-class image dataset for computer aided gastrointestinal disease detection," in *Proc. 8th ACM Multimedia Syst. Conf.*, Jun. 2017, pp. 164–169.
[38] D. J. C. Barbosa, J. Ramos, J. H. Correia, and C. S. Lima, "Automatic detection of small bowel tumors in capsule endoscopy based on color curvelet covariance statistical texture descriptors," in *Proc. Annu. Int. Conf. IEEE Eng. Med. Biol. Soc.*, Sep. 2009, pp. 6683–6686.
[39] M. Hajabdollahi, R. Esfandiarpoor, S. M. R. Soroushmehr, N. Karimi, S. Samavi, and K. Najarian, "Segmentation of bleeding regions in wireless capsule endoscopy images an approach for inside capsule video summarization," 2018, *arXiv:1802.07788*. [Online]. Available: http://arxiv.org/abs/1802.07788
[40] B. Münzer, K. Schoeffmann, and L. Böszörmenyi, "Content-based processing and analysis of endoscopic images and videos: A survey," *Multimedia Tools Appl.*, vol. 77, no. 1, pp. 1323–1362, Jan. 2018.
[41] L. A. D. Souza, L. C. S. Afonso, C. Palm, and J. P. Papa, "Barrett's esophagus identification using optimum-path forest," in *Proc. 30th SIBGRAPI Conf. Graph., Patterns Images (SIBGRAPI)*, Oct. 2017, pp. 308–314.
[42] O. H. Maghsoudi, M. Alizadeh, and M. Mirmomen, "A computer aided method to detect bleeding, tumor, and disease regions in wireless capsule endoscopy," in *Proc. IEEE Signal Process. Med. Biol. Symp. (SPMB)*, Dec. 2016, pp. 1–6.
[43] F. Deeba, M. Islam, F. M. Bui, and K. A. Wahid, "Performance assessment of a bleeding detection algorithm for endoscopic video based on classifier fusion method and exhaustive feature selection," *Biomed. Signal Process. Control*, vol. 40, pp. 415–424, Feb. 2018.
[44] K. He, J. Sun, and X. Tang, "Single image haze removal using dark channel prior," *IEEE Trans. Pattern Anal. Mach. Intell.*, vol. 33, no. 12, pp. 2341–2353, Dec. 2011.
[45] R. T. Tan, "Visibility in bad weather from a single image," in *Proc. IEEE Conf. Comput. Vis. Pattern Recognit.*, Jun. 2008, pp. 1–8.
[46] M.-M. Cheng, N. J. Mitra, X. Huang, P. H. S. Torr, and S.-M. Hu, "Global contrast based salient region detection," *IEEE Trans. Pattern Anal. Mach. Intell.*, vol. 37, no. 3, pp. 569–582, Mar. 2015.
[47] M. Sharif, M. A. Khan, Z. Iqbal, M. F. Azam, M. I. U. Lali, and M. Y. Javed, "Detection and classification of citrus diseases in agriculture based on optimized weighted segmentation and feature selection," *Comput. Electron. Agricult.*, vol. 150, pp. 220–234, Jul. 2018.
[48] M. A. Khan, T. Akram, M. Sharif, M. Y. Javed, N. Muhammad, and M. Yasmin, "An implementation of optimized framework for action classification using multilayers neural network on selected fused features," *Pattern Anal. Appl.*, vol. 22, no. 4, pp. 1377–1397, Nov. 2019.
[49] M. Rashid, M. A. Khan, M. Sharif, M. Raza, M. M. Sarfraz, and F. Afza, "Object detection and classification: A joint selection and fusion strategy of deep convolutional neural network and SIFT point features," *Multimedia Tools Appl.*, vol. 78, no. 12, pp. 15751–15777, Jun. 2019.

[50] H. Arshad, M. A. Khan, M. Sharif, M. Yasmin, and M. Y. Javed, "Multi-level features fusion and selection for human gait recognition: An optimized framework of Bayesian model and binomial distribution," *Int. J. Mach. Learn. Cybern.*, vol. 10, no. 12, pp. 3601–3618, 2019.
[51] M. A. Khan, M. Sharif, T. Akram, M. Raza, T. Saba, and A. Rehman, "Hand-crafted and deep convolutional neural network features fusion and selection strategy: An application to intelligent human action recognition," *Appl. Soft Comput.*, vol. 87, Feb. 2020, Art. no. 105986.
[52] S. A. Khan, M. Nazir, M. A. Khan, T. Saba, K. Javed, A. Rehman, T. Akram, and M. Awais, "Lungs nodule detection framework from computed tomography images using support vector machine," *Microsc. Res. Technique*, vol. 82, no. 8, pp. 1256–1266, Aug. 2019.
[53] Athi. (2019). *Texture Feature Extraction—GLDM*. MATLAB Central File Exchange. Accessed: Dec. 25, 2019. [Online]. Available: https://www.mathworks.com/matlabcentral/fileexchange/25057-texture-feature-extraction-gldm)
[54] G. Xu, Q. Cui, X. Shi, H. Ge, Z.-H. Zhan, H. P. Lee, Y. Liang, R. Tai, and C. Wu, "Particle swarm optimization based on dimensional learning strategy," *Swarm Evol. Comput.*, vol. 45, pp. 33–51, Mar. 2019.
[55] M. Z. Anwar, Z. Kaleem, and A. Jamalipour, "Machine learning inspired sound-based amateur drone detection for public safety applications," *IEEE Trans. Veh. Technol.*, vol. 68, no. 3, pp. 2526–2534, Mar. 2019.

MUHAMMAD ATTIQUE KHAN received the master's degree in human activity recognition for application of video surveillance from COMSATS University Islamabad, Pakistan, where he currently pursuing the Ph.D. degree. He is also a Lecturer at the Computer Science Department, HITEC University, Taxila, Pakistan. His primary research interests include medical imaging, MRI analysis, video surveillance, human gait recognition, and agriculture plants. He has above 50 publications that have more than 700 citations with H-index of 16. He is a reviewer of several reputed journals, such as the IEEE TRANSACTIONS ON INDUSTRIAL INFORMATICS, the IEEE TRANSACTIONS ON NEURAL NETWORKS AND LEARNING SYSTEMS, *Pattern Recognition Letters*, *Multimedia Tools and Applications*, *Computers and Electronics in Agriculture*, *IET Image Processing*, *IET Computer Vision*, *EURASIP Journal on Image and Video Processing*, and IEEE ACCESS.

SEIFEDINE KADRY (Senior Member, IEEE) received the bachelor's degree in applied mathematics from Lebanese University, in 1999, the M.S. degree in computation from Reims University, France, and EPFL, Lausanne, in 2002, the Ph.D. degree from Blaise Pascal University, France, in 2007, and the H.D.R. degree in engineering science from Rouen University, in 2017. He is currently working as an Associate Professor with Beirut Arab University, Lebanon. His current research interests include education using technology, smart cities, system prognostics, stochastic systems, and probability and reliability analysis. He is a Fellow of IET and ACSIT, and a Program Evaluator of ABET.

MAJED ALHAISONI is currently a Professor of computer science at University of Ha'il, Saudi Arabia. His research interest includes artificial intelligence and optimization. He has published more than 50 high impact factor articles in last three years. He is also a reviewer of many journals, such as *Multimedia Systems*, *Multimedia Tools and Applications*, and the IEEE TRANSACTIONS ON PATTERN ANALYSIS AND MACHINE INTELLIGENCE.

YUNYOUNG NAM (Member, IEEE) received the B.S., M.S., and Ph.D. degrees in computer engineering from Ajou University, South Korea, in 2001, 2003, and 2007, respectively. From 2007 to 2010, he was a Senior Researcher with the Center of Excellence in Ubiquitous System. From 2010 to 2011, he was a Research Professor with Ajou University. He was also a Postdoctoral Researcher at the Center of Excellence for Wireless and Information Technology, Stony Brook University, NY, USA, from 2009 to 2013. From 2013 to 2014, he was a Postdoctoral Fellow with Worcester Polytechnic Institute, Worcester, MA, USA. In 2017, he was the Director of the ICT Convergence Rehabilitation Engineering Research Center, Soonchunhyang University, where he is currently an Assistant Professor with the Department of Computer Science and Engineering. His research interests include multimedia database, ubiquitous computing, image processing, pattern recognition, context-awareness, conflict resolution, wearable computing, intelligent video surveillance, cloud computing, biomedical signal processing, rehabilitation, and healthcare systems.

YUDONG (EUGENE) ZHANG (Senior Member, IEEE) held a postdoctoral position at Columbia University, from 2010 to 2012. From 2012 to 2013, he worked as an Assistant Research Scientist at Columbia University and at the New York State Psychiatric Institute. From 2013 to 2017, he was a Full Professor and Doctoral Advisor at the School of Computer Science and Technology, Nanjing Normal University. He also serves as the Academic Leader of the "Jiangsu Key Laboratory of 3D Printing Equipment and Manufacturing." He is currently a Professor of knowledge discovery and machine learning at the Department of Informatics, University of Leicester, U.K. His research interests include computer-aided medical diagnosis and biomedical image processing.

VENKATESAN RAJINIKANTH received the Ph.D. degree in the field of heuristic algorithms from Anna University, India, in 2013. He is currently working as a Professor at the Department of EIE, St. Joseph's College of Engineering, Chennai, India. He has published over 80 articles in the field of heuristic algorithms and its applications. His research interests include heuristic algorithm assisted medical image processing, signal processing, and controller design.

MUHAMMAD SHAHZAD SARFRAZ (Member, IEEE) is currently an Associate Professor of computer science at the FAST-National University of Computer and Emerging Sciences. He served as an Associate Professor, the Chairperson of Computer Science, and the Director of the Evening Programs at the University of Gujrat and at the COMSATS Institute of Information Technology, and also an Assistant Professor at the Department of Computer Science, NUCES. He was a Ph.D. Scholar and a Teaching/Research Associate at the Asian Institute of Technology (AIT), Thailand, and a Visiting Researcher at the Digital Image Processing Lab, National Institute of Informatics (NII), Tokyo, Japan. He has extensive background and interest in using geospatial technologies to strengthen and integrate health systems. He contributed in many seminars/workshops, organized at national and international levels, which supported collaborative research in ten countries. He is a member of numerous international societies, like Telecoms Sans Frontieres for emergency response in Asia-Pacific, ISPRS Health, Geological Society of America, International Medical Geological Association, eHealth Association of Pakistan, and American Telemedicine Association.